JOURNAL OF EXPERIMENTAL NANOSCIENCE, 2017
https://doi.org/10.1080/17458080.2017.1321794

Taylor & Francis
Taylor & Francis Group

Bioinspired study of energy and electron transfer in photovoltaic system

Md Moniruddin[a*], Baurzhan Ilyassov[b*], Evgeniya Seliverstova[c*], Yerkin Shabdan[d], Nurlan Bakranov[e], Niyazbek Ibrayev[c] and Nurxat Nuraje[a]

[a]Department of Chemical Engineering, Texas Tech University, Texas, TX, USA; [b]Laboratory of Solar Energy, PINLA, Nazarbayev University, Astana, Kazakhstan; [c]Department of Physics, Buketov Karaganda State University, Karaganda, Kazakhstan; [d]Department of Physics and Technology, Al-Farabi Kazakh National University, Almaty, Kazakhstan; [e]Department of Physics, Kazakh National Technical University, Almaty, Kazakhstan

ABSTRACT

This study focuses on understanding the fundamentals of energy transfer and electron transport in photovoltaic devices with uniquely designed nanostructures by analysing energy transfer in purple photosynthetic bacteria using dye-sensitised solar cell systems. Förster resonance energy transfer between the xanthene dye (donor of energy) and a new polymethine dye (acceptor of energy) was studied in dye-sensitised solar cells, which leads to a doubling of energy conversion efficiency in comparison to the cell with only the polymethine dye. The electron transport in the two different nanostructures of zinc oxide (nanorods and nanosheets) was investigated by spectroscopic methods (UV-vis spectrometer, time-resolved photoluminescence spectroscopy) and electrochemical potentiostat methods. The nanosheet structure of zinc oxide showed high short circuit current and long diffusion length. This fundamental study will lead to efficient artificial photosystem designs.

ARTICLE HISTORY
Received 5 March 2017
Accepted 15 April 2017

KEYWORDS
Photovoltaic; nanostructure; FRET

1. Introduction

Commercialisation of solar cells requires efficiency, stability, cost effectiveness and material availability. At present, a solar cell which could fulfil all these criteria still requires improvement of the existing technology and the development of new pathways by alternative mechanisms for solar energy conversion [1–4].

One promising area is the dye-sensitised solar cell (DSSC), which utilises a Ru-dye similar to plant chlorophyll, and applies a self-assembly principle, which reduces process costs [5–8]. Although DSSC is a special type of the solar cells and demonstrates power conversion efficiency up to 13%, the availability of Ru-dyes and the stability of liquid-based electrolytes are still the main concerns when developing this type of solar cell [9–14].

CONTACT Niyazbek Ibrayev niazibraev@mail.ru; Nurxat Nuraje nurxat.nuraje@ttu.edu
* These authors contributed equally
Supplemental data for this article can be accessed http://dx.doi.org/10.1080/17458080.2017.1321794.

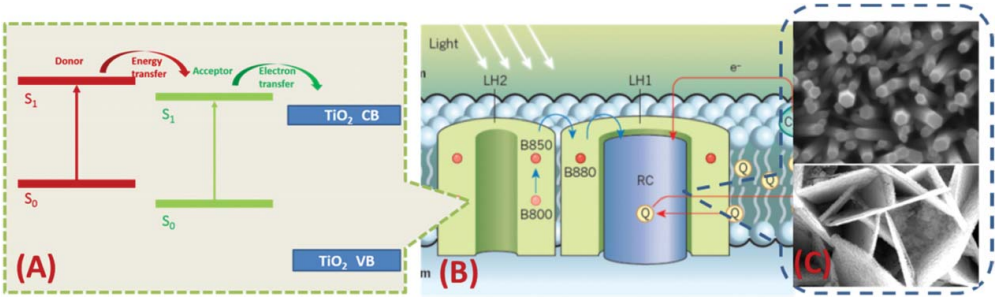

Figure 1. (A) Scheme explaining FRET system consisting of xanthene dye and a polymethine dye on the titania film; (B) Scheme for energy and electron transfer in purple bacteria membrane including light harnessing I(LH-I), light harnessing II(LH-II), and reaction centre. (C) ZnO morphology with nanorod and nanosheet existed in purple bacteria membrane for electron transfer.

Natural photosynthetic systems are the result of perfectly assembled and efficient systems of natural dyes coupled with protein molecules that harvest sunlight and use its energy to drive metabolic reactions [15]. The solar energy conversion process includes critical steps of solar energy harnessing, charge separations and catalytic reaction. One of the strongest examples of this process is Purple photosynthetic bacteria [16] (Figure 1 (B)), which contain two types of light-harvesting complexes – light-harvesting complex I (LH-I) and light-harvesting complex II (LH-II) – and surround the reaction centre (RC) in the bacteria's photosynthetic membranes. This assembly system retains the distinctive structure of a photosynthetic complex with a new type of light-harvesting protein and transport channels that allow efficient energy and electron transfer. The excitation transfer from LH-II -⟶ LH-I -⟶ RC occurs within 100 picoseconds at about 95% efficiency [17,18]. B800 BChls, bacteriochlorophylls (BChls) which act as antennas with the carotenoids, absorb the sunlight at 800 nm and funnel its energy to the ring B850 BChls (absorbing light at 850 nm) through the Förster resonance energy transfer (FRET) mechanism [19,20]. By understanding the structure of light-harvesting complexes, we can advance our understanding of the primary excitation transfer process just as the structure of the RC revolutionised the study of the primary electron transfer processes. The arrangement of the main pigment-protein complexes, among LH-I and the photosynthetic RC explained by recent electron microscopy data, suggest that the hierarchy arrangement of the electron transfer system in RC is mostly shown as cylinders (or rods) and coplanar structures (sheets) [16]. Moreover, due to the elegant structure of the biological organism, genetically engineered viruses [21–23] were applied to the solar energy conversion system in order to study solar cell and water splitting.

Nanotechnology provides us with ways of building nanostructures as they exist in a natural photosynthetic system [17,24]. This study focuses on energy transfer and electron transport in a photovoltaic device coupled with uniquely designed nanostructures inspired by photosynthetic bacteria. A DSSC system provides a base for investigating fundamental problems including energy transfer and electron transport. In the study of electron transport properties, uniquely assembled nanostructures of ZnO were fabricated using electrochemical and chemical vapour deposition (CVD) approaches. The assembled nanostructures, including one-dimensional nanorods, and nanosheets, were investigated for electron transfer using characterisation methods (SEM, TEM and XRD), spectroscopic

methods such as UV-vis spectrometer and time-resolved photoluminescence spectroscopy, and electrochemical potentiostat methods. In the study of energy transfer, FRET between the xanthene dye (donor of energy) and a new polymethine dye (acceptor of energy) is studied on the surface of TiO_2 films by time-resolved photoluminescence spectroscopy, and this fundamental study will lead us to better designed artificial photosystems.

2. Experimental

2.1. Materials and methods

The organic dyes, rhodamine 6G and squarylium dye (SQ), were chosen, respectively, as the donor and acceptor of energy (**Supporting Figure 1**). Deionised water (DI water) was used to prepare all solutions. ZnO oxide nanomaterials with different morphologies were synthesised using the following procedures. N719 dye, ITO substrates, thermoplastic sealing spacer (Meltonix 1170-25, a 25 μm thick Solaronix) and electrolyte were purchased from Solaronix. Zinc acetate dehydrate [$(Zn(CH_3COO)_2{\cdot}2H_2O)$], monoethanolamine ($C_2H_7NO$) and hexamethylenetetramine ($C_6H_{12}N_4$) were purchased from Sigma-Aldrich.

2.2. Preparation of ZnO nanorods

Preparation of ZnO seed layers. To prepare ZnO seed layers, first 0.5 M of zinc acetate dehydrate [$(Zn(CH_3COO)_2{\cdot}2H_2O$, Sigma Aldrich)] in the mixed solution of monoethanolamine (C_2H_7NO, Sigma-Aldrich) and isopropyl alcohol was spin-coated onto ITO substrates at 3000 rpm five times [25]. Then, the ITO substrates were thermally heated at 400 °C in air for 30 minutes to transform zinc acetate to ZnO.

Hydrothermal deposition. To fabricate ZnO nanorods, the hydrothermal approach was applied to grow ZnO nanorods vertically via heating the ZnO-seeded ITO substrates in solutions of 25 mM $Zn(NO_3)_2$ (Sigma-Aldrich) and 25 mM hexamethylenetetramine ($C_6H_{12}N_4$, Sigma-Aldrich) at 90 °C for 10 hours. Finally, the resulting substrates were cleaned with water/ethanol and annealed at 400 °C for 30 minutes to eliminate any residual organics.

2.3. Preparation of ZnO nanosheets

In brief, in the synthesis of the ZnO nanosheets, an a three-electrode electrochemical configuration set up (consisting of an ITO substrate (working electrode), a graphite electrode (counter electrode) and a saturated Ag/AgCl (reference electrode), respectively) was applied to deposit the arrays of hexagonal $Zn_5(OH)_8Cl_2$ nanosheets first at −1.1 V and 50 °C conditions for 30 minutes in the aqueous electrolyte of 0.05M $Zn(NO_3)_2$ and 0.1M KCl . Subsequently, a pyrolytic transformation of $Zn_5(OH)_8Cl_2$ into ZnO nanosheets was performed at 400 °C in air.

2.4. Assembly of DSSC

Solar cells were prepared and assembled according to a previously described procedure [26]. Briefly, the prefabricated ZnO-based photoanodes, each with an active surface area

of 0.2 cm^2, were immersed in a dry ethanol solution containing 0.5 mM of N719 (Solaronix) at 50 °C for 1 h to load the dye at first. A Pt coated conductive glass substrate was applied as the counter electrode. The Pt layer was prepared on the ITO glass through electrodeposition approach as described elsewhere [27,28]. The DSSC was assembled by placing the Pt-coated counter electrode over the dyed ZnO-based photoanode separated by a 25 μm thick thermoplastic sealing spacer (Meltonix 1170-25, Solaronix). The cell's internal space was filled with a highly stable liquid electrolyte containing Iodolyte Z-150 (Solaronix; Redox couple: iodide/tri-iodide; redox concentration: 150 mM; additives: ionic liquid, alkylbenzimidazole, thiocyanate; solvent: 3-methoxypropionitrile).

3. Results and discussion

The two types of artificial mimicked photosystem were built and explored to understand FRET-energy transfer and electron transport properties based on the model of DSSC, respectively.

Designation of FRET-energy system and its study:

To mimic the FRET system in purple bacteria, a donor/acceptor system consisting of a xanthene dye (rhodamine as a donor) and a polymethine dye (squarylium dye (SQ) as acceptor) was selected for study. This system is located on the surface of TiO_2 films in the DSSC because of their higher molar extinction coefficients (100,000–300,000 M^{-1} cm^{-1}) than ruthenium-based complexes (low molar extinction coefficients (5000–20,000 $M^{-1}cm^{-1}$)) [29]. In order to prepare samples with proper concentrations of rhodamine and squarylium dye, the Förster critical distance and critical concentration (**Supporting Table 1**) were calculated to be 2.9 nm and 10^{-2} M based on the spectral measurement data [30,31]. The critical distance between these two dyes was determined to be 2.9 nm, which is in the range of the values of purple bacteria [16]. As shown in Figure 1(B), in the FRET energy system of a purple bacteria the absorption energy of donor dye (absorption of Bacteriochlorophylls (BChls), 'B800 BChls', at 800 nm) must be higher than that of the absorption energy of acceptor (absorption of B850 BChls at 850 nm) [16], where light-harvesting pigments transfer their energy to the RC. Figure 2(A) shows that the fluorescence spectrum of the donor and the absorption spectrum of the acceptor overlaps, a prerequisite for effective electronic excitation energy transfer. Absorbance of rhodamine 6G and squarylium dye (SQ) are 525 and 625 nm, respectively. Therefore, Rhodamine should efficiently transfer the energy by the Förster process to the anchored SQ. Time-resolved fluorescence spectroscopy was applied to measure the fluorescence decay kinetics in the absorption band of the donor using radiation from a laser with a wavelength (λ_{gen}) of 488 nm. Peaks of donor and acceptor fluorescence were found to be 555 and 660 nm, respectively. The concentrations of the donor and acceptor in these measurements were chosen under the critical concentration, the requirement for transferring the greatest amount of the excitation energy to acceptor molecules. .

Furthermore, FRET-energy transfer between rhodamine 6G and squarylium dye (SQ) (Table 1) was studied in TiO_2 films in comparison with a sole donor and a sole acceptor at various concentrations of components [32]. The efficiency of energy transfer, E_{ET}, was calculated according to the reference [33].

As shown in Table 1, the excited-state lifetime of the donor in the presence of acceptor molecules decreases with increasing concentration of the acceptor molecules. The lifetime

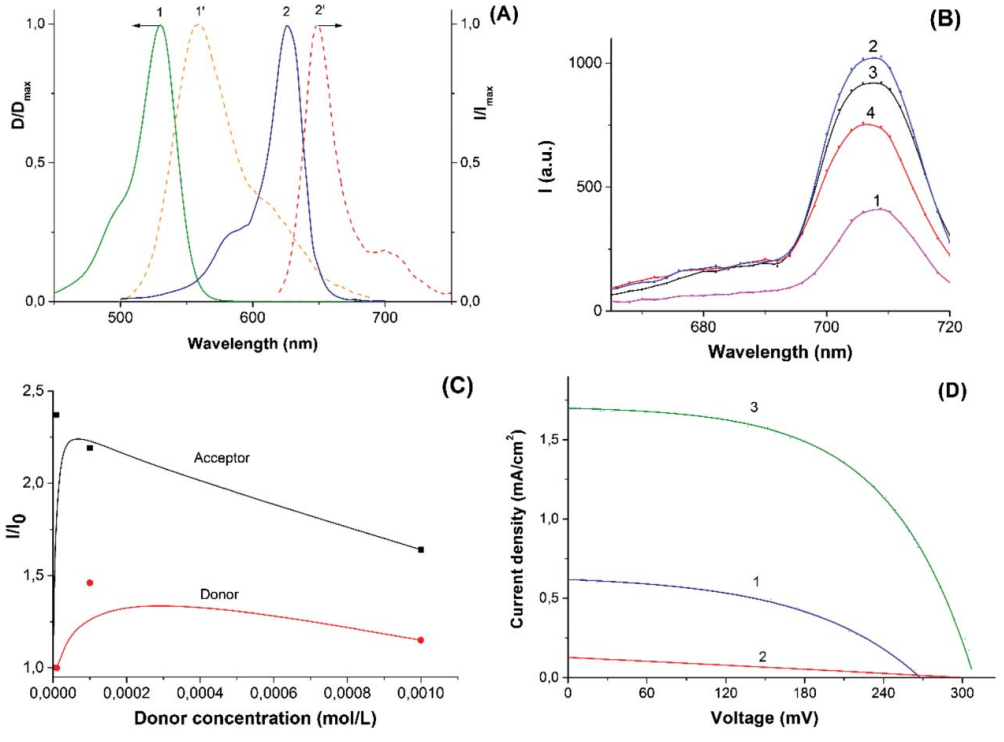

Figure 2. (**A**) Normalised absorption (1,2) and fluorescence (1',2') spectra of donor (rhodamine: 1,1') and acceptor (squarylium dye (SQ):2,2') at concentration C = 10^{-5} mol/L. (**B**) Fluorescence spectra of TiO_2 films sensitised by the acceptor(squarylium dye (SQ): (1) at the concentration of 10^{-4} mol/L and the donor of energy (rhodamine) at various concentrations in the donor and acceptor mixture (mol/L): (2) – 10^{-3}; (3) – 10^{-5}; (4) – 10^{-4}. Films are illuminated with white light. **(C)** Normalised intensity of donor (λ_{reg} = 565 nm) and the acceptor (λ_{reg} = 710 nm) via donor concentration**. (D)** A current-voltage curve of solar cells sensitised by the only acceptor molecules (squarylium dye) (curve 1), by the only donor (rhodamine) (curve 2) and by the donor-acceptor system (curve 3) at donor concentration of 10^{-5} mol/L.

of acceptor molecules has a value close to the lifetime of the donor, which confirms the implementation of the process of energy transfer between the selected dyes and reaches the highest energy transfer.

Likewise, the fluorescence intensity of the acceptor (in the presence of, and without donor molecules, under illumination by a xenon lamp) was also measured to evaluate their effects on the performance of the cell – co-sensitisation of TiO_2 semiconductor film by the donor and acceptor molecules. Figure 2(B) indicated the luminescence intensity of

Table 1. Fluorescence lifetime of energy donor and acceptor adsorbed onto TiO_2 films (λ_{reg} : wavelength; τ(ns): fluorescence lifetime life time; E_{ET}: efficiency of energy transfer E_{ET}).

	τ (ns)		
Donor-acceptor concentration, mol/L	λ_{reg} = 555 nm	λ_{reg} = 660 nm	E_{ET}
Donor	1.1 (ns)	1.1 (ns)	-
Acceptor	0.7 (ns)	0.7 (ns)	-
10^{-5}; 10^{-6}	1.1 (ns)	1.0 (ns)	0
10^{-5}; 10^{-5}	0.9 (ns)	0.95 (ns)	0.19
10^{-5}; 10^{-4}	0.8 (ns)	0.8 (ns)	0.28

the acceptor is 2.5 times high as that of sole acceptor. Addition of donor molecules or acceptor molecules with respect to one another leads to the quenching of fluorescence of rhodamine or polymethine dyes in respective measurements: this explains efficient FRET energy transfer between donor and acceptor molecules in the presence of titania assembled films [34]. Figure 2(C) shows the strong photoluminescence at the low concentration range for both donor and acceptor.

The quenching of the fluorescence intensity of dyes at the growth of donor concentration is the result of molecular aggregation of rhodamine dye. The strongest quenching for both donor and acceptor were equal to about 25% and registered at donor concentration of 10^{-3} mol/L. After identifying the correct ratio between donor and acceptor molecules in the porous titania films, the conversion of light energy into electrical energy in the DSSC solar cells was investigated further. The energy conversion efficiency of the semiconductor films sensitised by the donor–acceptor compound was evaluated in parallel study with either the sole squarylium dye (SQ) or rhodamine 6G measured by solar cell tester and potentiostat.

Figure 2(D) shows a current-voltage curve for solar cells sensitised by SQ dye molecules, (curve 1), sole donor molecules (curve 2) and donor-acceptor compound (curve 3). I_{sc} of solar cells with only SQ, and sole rhodamine was equal to 0.62 and 0.12 mA/cm^2. In the case of co-sensitisation of the solar cell with donor and acceptor at the above ratio, the I_{sc} value was significantly increased to 1.7 mA/cm^2. The power conversion efficiency of TiO_2 solar cells consisting of donor-acceptor is more than 2.5 times over a pristine cell. The optimum concentration of donor molecules for the co-sensitisation of solar cell is 10^{-5} mol/L.

The curves of spectral photosensitivity of solar cell indicated (**Supporting Figure 2**) that the photosensitivity for the donor-acceptor system had a higher photosensitivity than that of the sole acceptor which supported the I-V curve results.

Study of nature-inspired electron transport system:

In designing electron transport pathways for mimicking photosynthetic purple bacteria (Figure 1(B,C)), ZnO nanostructures with rods and sheets were selected, since ZnO with different nanostructures is easily fabricated, has a better electron mobility, and similar band gap structure with titania [35]. These nanostructures were main aggregate forms in the electron transport pathways in the RC and LH-I of purple bacteria. ZnO's nanorods and nanosheets were synthesised by both hydrothermal and electrochemical deposition methods, respectively, and are confirmed by scanning electron microscopy (SEM) (Figure 3(a,b)). Figure 3(c,d) indicated that nanorods and nanosheets possess wurtzite crystal structure. A unique crystal face (0001) in the nanosheet structure of zinc oxide is considered to be a polar plane. The influence of the polar plane, defect density and morphology of these nanostructures on photovoltaic and electron transport properties was evaluated by the following approaches: photoluminescence study, electrochemical impedance spectroscopy and analysis of dye-loading amount in the photoelectrodes in parallel with solar cell performance measurement. Photovoltaic performance of the DSSC cells constructed from nanorod and nanosheet arrays was listed in presence of the highly stable electrolytes, including the high boiling organic solvent and a mixture of ionic liquids with relatively low viscosity, using Ru-dye (N719) in Table 2 and Figure 4(A).

Figure 4(A) indicated that the short-circuit current density (J_{sc}) of the nanosheet array (NSh cell) cell is almost five to six times more than that of the nanorod array (NR cell)-based cell,

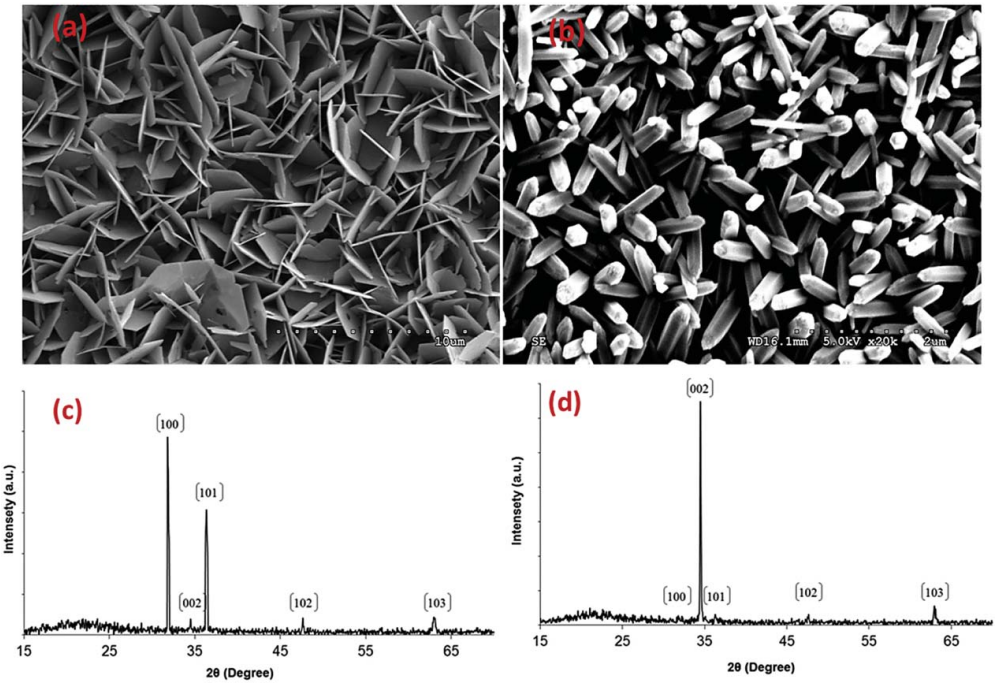

Figure 3. SEM images of arrays of (a) ZnO nanosheet (on the left) and (b) nanorod (on the right). X-ray diffraction spectra of (c) ZnO nanorods and (d) nanosheets.

whereas, the open circuit voltage (V_{OC}) of the NSh cell is the opposite. In addition, the fill factor (FF) of the NSh cell is significantly lower than that of the NR cell. Since the same dye (N719) was utilised in the solar cell test, the big difference in the J_{sc} of the two cells is due to different surface areas and different light scattering properties. One possible explanation is that the nanosheet structure has a feature size close to the light wavelength and may generate stronger light scattering, thus increasing the current density, a point that needs further confirmation. Another possible explanation is that the photoexcited electrons inject more efficiently from the dye molecules into ZnO through the polar face of ZnO since ZnO brings a large surface to the nanosheet array.

To prove the idea, the amount of the dye loaded in both structures was evaluated by UV-vis absorption measurement after desorbing the dye molecules from ZnO film in the base solution. The dye absorption spectrum of nanosheet array is significantly larger than that of nanorod array (**Supporting Figure 3**), which indirectly suggests that surface area of a nanosheet array is larger than that of a nanorod array.

The defect density of the zinc oxide is also one of the factors that could significantly affect the cell photovoltage. The photovoltage is determined by the increase of the quasi-

Table 2. Photovoltaic performances of DSSCs consisting of the nanorod and nanosheet arrays of ZnO and electron transport properties of ZnO nanostructures estimated by EIS analyses.

	Thickness (μm)	J_{SC}(mA/cm^2)	V_{OC}(V)	FF	T_{eff}(μs)	n_s(cm^{-3})
NSh-DSSC	4.2	0.68	0.66	0.52	3.94	4.86×10^{16}
NR-DSSC	3.3	3.72	0.37	0.36	3.69	1.39×10^{16}

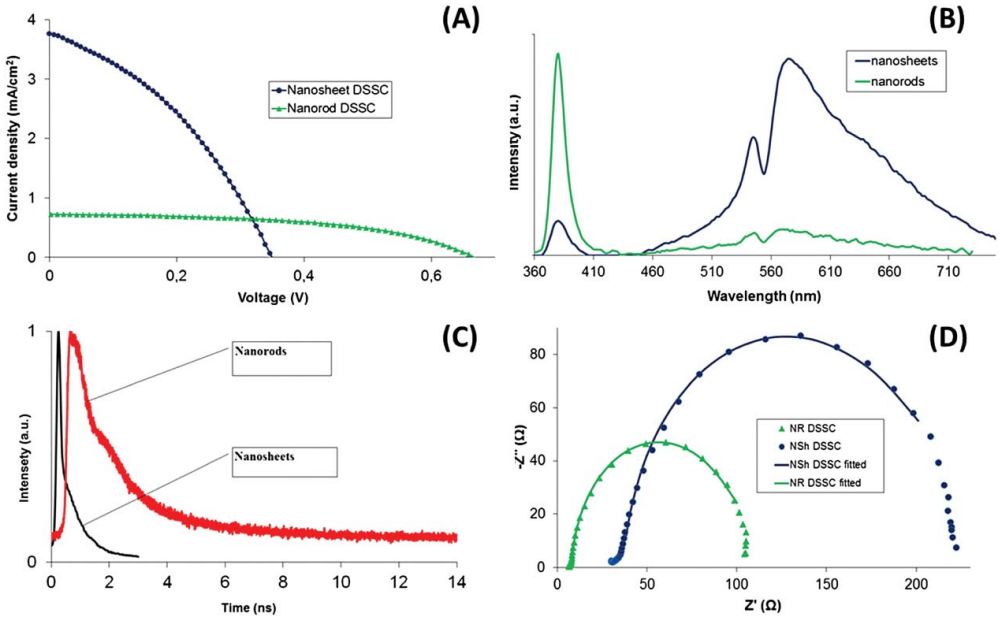

Figure 4. (Colour online). (A) Current-voltage characteristic of DSSCs based on the ZnO nanorod (green line) and nanosheet (blue line) arrays. (B) The normalised PL spectra of nanosheet (blue line) and nanorod (green line) arrays of ZnO. (C) Decay kinetics of the edge luminescence band (ELB) of the ZnO nanorods (red line) and nanosheets (blue line). (D) Nyquist plots of DSSCs performed under illumination at the applied bias of V_{oc}. The solid lines are the fitting results from the equivalent circuit model of ZnO DSSCs.

Fermi level of the semiconductor, E_{Fn}, under a constant illumination with respect to the dark value, E_{F0}, which equals the electrolyte redox energy [36]. Another way of understanding this is that defects can trap the excited electrons and diminish the concentration of the injected electron in the conduction band of the semiconductor. As shown in Equation (1), the quasi-Fermi level of the semiconductor is proportional to the electron concentration in the conduction band, n [36]:

$$V_{OC} = E_{Fn} - E_{F0} = (k_B T/e) Ln\left(\frac{n}{n0}\right) \quad (1)$$

Therefore, the low value of V_{OC} of NSh in comparison with V_{OC} of the NR cell may be related to the effect of defects, which was confirmed by the photoluminescence (PL) properties of nanosheets and nanorods (Figure 4 (B)). The PL spectra of nanosheets (blue line) and nanorods (green line) (Figure 4 (B)) showed a sharp emission peak at 380 nm and a broad band with two peaks centred at 546 and 576 nm. The UV emission at 380 nm is ascribed to recombination of the free excitations or near band edge emission of the wide band-gap ZnO [36,37] and the visible light emission is related to defects, due to oxygen vacancies or zinc interstitials [38,39]. Furthermore, the black line exhibits a very strong UV emission and a negligible visible emission, while the red line shows a relatively strong visible emission. Their ratios of UV/visible emissions are 7.7 and 0.17 under our current measurement conditions, respectively. This result indicates that the nanosheets have

much more defect density, or it is due to the different disorder or defects located at different crystal planes [40,41]. Figure 4(C) shows the kinetics of the edge luminescence band (ELB) decay for the nanorods and nanosheets. The ELB of ZnO decays in the subnanosecond range [42]. As can be seen from Figure 4(C), the decay kinetics of ELB for both the nanorods and nanosheets is a nonexponential function. The lifetimes calculated from these curves are ~1.1 and 2.33 ns for the nanorods and 0.71 and 1.7 ns for the nanosheets. As can be seen, the ELB of nanosheets decays faster than that of the nanorods.

In the DSSCs based on TiO_2 films, the majority of the photoinjected electrons are located in trap states in the nanostructured TiO_2 film [43,44], leading to a trapped electron density that greatly exceeds the conduction electron density. These electrons must be released thermally to the conduction band before they can reach the interface and transfer to I^{3-} ions. These trapping and detrapping transport models of photoinjected electrons have been confirmed by the data of electrical impedance spectroscopy (EIS), intensity-modulated photovoltage spectroscopy (IMVS) and photovoltage decay measurements [43–45].

Electron transport properties in the DSSC cells were further investigated by considering the parameters: two different morphologies and a defect density of the ZnO nanostructures by electrochemical impedance spectroscopy (EIS). The results were further analysed by the general transmission line model of ZnO nanostructured DSSCs based on the diffusion-recombination model proposed by Bisquert [46]. The Nyquist plots for impedance data of the NSh and NR cells and the fitting results are shown in Figure 4(D) and the related electron transport parameters were obtained from the Nyquist plots according to the reference [47]. The results show that electron densities at the steady state (n_s) in the conduction band of NSh-ZnO cell are approximately three to four times larger than these of NR- ZnO cell and indicated that larger number of electrons are injected in NSh, which are consistent with high J_{SC}. Furthermore, the effective electron lifetime (τ_{eff}) of NSh ZnO cell is higher than that of NR ZnO cell. As discussed in references [48,49], the electron diffusion length ($L_n = (D^*\tau_{eff})^{1/2}$ is proportional to $(\tau_{eff})^{1/2}$. The collection diffusion length, L_c, determines the short circuit current of a solar cell which is illuminated with light of near-bandgap wavelength [50,51]. Therefore, the high electron density and longer electron life time in NSh-ZnO cell are to some degree explain the high short circuit current of the cell.

4. Conclusions

In this paper, we investigated the FRET-energy transfer between molecules of rhodamine and polymethine dye in TiO_2 films and electron transport in different nanostructures of zinc oxides.

The fluorescence decay kinetics of the energy donor revealed a reduction of the excited state lifetime of the donor in the presence of acceptor molecules and confirmed that the efficiency of energy transfer was 22% at an acceptor molecule concentration of 10^{-4} mol/L. Under white light illumination, the intensity of sensitised fluorescence of polymethine was almost doubled and its photovoltaic efficiency of solar cells was increased 2.5 times in the presence of rhodamine dye molecules. The main reason for the increase of the cell's efficiency is connected to the energy transfer process. These results are very important to

understanding and completing the assembly of high efficient solar cells sensitised with organic dyes.

In addition, we studied the effect of ZnO nanorod and nanosheet on the solar cell efficiency of DSSCs. The nanosheets have a larger defect structure than the nanorods, which was confirmed by a relatively strong visible/defect emission. The short current of DSSC made of ZnO nanosheet was five to six times larger than that of the DSSC with nanorods. This observation is supported by two explanations: first, that nanosheet structures have more dye loading in contrast to nanorod structures, which was confirmed by the UV-vis absorption spectra of desorbed dye molecules; the second is that the nanosheet structure of zinc oxide possesses a relatively high electron density and an effective long electron life time in the NSh-ZnO cell in contrast to the NR-ZnO cell. However, we also consider the possibility that the electron photoinjection from the dye molecules into ZnO more effectively occurs through the ZnO polar plane (0001), making the dominant contribution to the surface area of the nanosheets, unlike the nanorods. The low photovoltage of DSSC with the nanosheet array was due to the low electron trap density, which can reduce the electron quasi-Fermi level. .

Acknowledgment

This work was supported by the Texas Tech Start-up Fund and ACS PRF Grant (PRF#57095-DNI7).

Disclosure statement

The authors declare no competing financial interests.

Funding

American Chemical Society Petroleum Research Fund [grant number PRF# 57095-DNI7]; Texas Tech Start-up Fund.

References

[1] Polman A, Knight M, Garnett EC, et al. Photovoltaic materials: present efficiencies and future challenges. Science. 2016;352:307–317.
[2] Boghossian AA, Ham M-H, Choi JH, et al. Biomimetic strategies for solar energy conversion: a technical perspective. Energ Environ Sci. 2011;4:3834–3843.
[3] Maennig B, Drechsel J, Gebeyehu D, et al. Organic p-i-n solar cells. Appl Phys A: Mater Sci Process. 2004;79:1–14.
[4] Hiramoto M, Fujiwara H, Yokoyama M. 3-layered organic solar-cell with a photoactive interlayer of codeposited pigments. Appl Phys Lett. 1991;58:1062–1064.
[5] Hardin BE, Hoke ET, Armstrong PB, et al. Increased light harvesting in dye-sensitized solar cells with energy relay dyes. Nat Photon. 2009;3:406–411.
[6] Morisue M, Yamatsu S, Haruta N, et al. Surface-grafted multiporphyrin arrays as light-harvesting antennae to amplify photocurrent generation. Chem A European J. 2005;11:5563–5574.
[7] Lee CY, Hupp JT. Dye sensitized solar cells: TiO2 sensitization with a bodipy-porphyrin antenna system. Langmuir. 2010;26:3760–3765.

[8] Odobel F, Pellegrin Y, Warnan J. Bio-inspired artificial light-harvesting antennas for enhancement of solar energy capture in dye-sensitized solar cells. Energ Environ Sci. 2013;6:2041–2052.
[9] Kang S, Umeyama T, Ueda M, et al. Ordered supramolecular assembly of porphyrin-fullerene composites on nanostructured SnO2 electrodes. Adv Mater. 2006;18:2549–2552.
[10] Gratzel M. Photoelectrochemical cells. Nature. 2001;414:338–344.
[11] Gratzel M. Conversion of sunlight to electric power by nanocrystalline dye-sensitized solar cells. J Photochem Photobiol A Chem. 2004;164:3–14.
[12] Gao F, Wang Y, Zhang J, et al. A new heteroleptic ruthenium sensitizer enhances the absorptivity of mesoporous titania film for a high efficiency dye-sensitized solar cell. Chem Commun. 2008;23:2635–2637.
[13] Gao F, Wang Y, Shi D, et al. Enhance the optical absorptivity of nanocrystalline TiO(2) film with high molar extinction coefficient ruthenium sensitizers for high performance dye-sensitized solar cells. J Am Chem Soc. 2008;130:10720–10728.
[14] Mathew S, Yella A, Gao P, et al. Dye-sensitized solar cells with 13% efficiency achieved through the molecular engineering of porphyrin sensitizers. Nat Chem. 2014;6:242–247.
[15] Nuraje N, Moniruddin MD, Kudaibergenov S. Hierarhical nanoheterostructures for water splitting. In: Nuraje N, Asmatulu R, Mul G, editors. Green photo-active nanomaterials: sustainable energy and environmental remediation. London: The Royal Society of Chemistry; 2015. p. 142–167.
[16] Hu X, Schulten K. How nature harvests sunlight. Physics Today. 1997;50:28–34.
[17] Pullerits T, Sundström V. Photosynthetic light-harvesting pigment—protein complexes: toward understanding how and why. Acc Chem Res. 1996;29:381–389.
[18] van Grondelle R, Dekker JP, Gillbro T, et al. Energy transfer and trapping in photosynthesis. Biochim et Biophys Acta (BBA) - Bioenerg. 1994;1187:1–65.
[19] Oppenheimer JR. On the interaction of mesotrons and nuclei. Phys Rev. 1941;60:150–158.
[20] Arnold W, Oppenheimer JR. Internal conversion in the photosynthetic mechanism of blue-green algae. J Gen Phys. 1950;33:423–435.
[21] Nam YS, Magyar AP, Lee D, et al. Biologically templated photocatalytic nanostructures for sustained light-driven water oxidation. Nat Nano. 2010;5:340–344.
[22] Dang X, Yi H, Ham M-H, et al. Virus-templated self-assembled single-walled carbon nanotubes for highly efficient electron collection in photovoltaic devices. Nat Nano. 2011;6:377–384.
[23] Nuraje N, Dang X, Qi J, et al. Biotemplated synthesis of perovskite nanomaterials for solar energy conversion. Adv Mater. 2012;24:2885–2889.
[24] Ilyassov B, Ibrayev N, Nuraje N. Hierarchically assembled nanostructures and their photovoltaic properties. Mater Sci Semicond Process 2015;40:885–889.
[25] Kamaruddin SA, Chan K-Y, Yow H-K, et al. Zinc oxide films prepared by sol–gel spin coating technique. Appl Phys A. 2011;104:263–268.
[26] Ito S, Murakami TN, Comte P, et al. Fabrication of thin film dye sensitized solar cells with solar to electric power conversion efficiency over 10%. Thin Solid Films. 2008;516:4613–4619.
[27] Lee KS, Lee HK, Wang DH, et al. Dye-sensitized solar cells with Pt- and TCO-free counter electrodes. Chem Commun. 2010;46:4505–4507.
[28] Gao Y, Chu L, Wu M, et al. Improvement of adhesion of Pt-free counter electrodes for low-cost dye-sensitized solar cells. J Photochem Photobiol A Chem. 2012;245:66–71.
[29] Hu H, Przhonska OV, Terenziani F, et al. Two-photon absorption spectra of a near-infrared 2-azaazulene polymethine dye: solvation and ground-state symmetry breaking. Phys Chem Chem Phys. 2013;15:7666–7678.
[30] Jankowski D, Bojarski P, Kwiek P, et al. Donor–acceptor nonradiative energy transfer mediated by surface plasmons on ultrathin metallic films. Chem Phys. 2010;373:238–242.
[31] Förster Th. Zwischenmolekulare Energiewanderung und Fluoreszenz [Intermolecular energy migration and fluorescence]. Ann Phys. 1948;437:55–75.
[32] Siegers C, Hohl-Ebinger J, Zimmermann B, et al. A dyadic sensitizer for dye solar cells with high energy-transfer efficiency in the device. Chem Phys Chem. 2007;8:1548–1556.

[33] Ermolayev VL, Sveshnikova LV, Shakhveredov TA, et al. Nonradiative energy transfer of electron excitation. Leningrad: USSR; 1977. Russian.
[34] Yeroshina SA, Ibrayev NK, Kudaibergenov SE, et al. Spectroscopic properties of mixed Langmuir–Blodgett films of rhodamine dyes and poly(N,N-diallyl-N-octadecylamine-alt-maleic acid). Thin Solid Films. 2008;516:2109–2114.
[35] Ghicov A, Schmuki P. Self-ordering electrochemistry: a review on growth and functionality of TiO2nanotubes and other self-aligned MOx structures. Chem Commun. 2009:2791–2808.
[36] Segawa Y, Ohtomo A, Kawasaki M, et al. Growth of ZnO thin film by laser MBE: lasing of exciton at room temperature. Physica Status Solidi (B). 1997;202:669–672.
[37] Wu JJ, Liu SC. Low-temperature growth of well-aligned ZnO nanorods by chemical vapor deposition. Adv Mater. 2002;14:215–218.
[38] Vanheusden K, Seager CH, Warren WL, et al. Correlation between photoluminescence and oxygen vacancies in ZnO phosphors. Appl Phys Lett. 1996;68:403–405.
[39] Korsunska NO, Borkovska LV, Bulakh BM, et al. The influence of defect drift in external electric field on green luminescence of ZnO single crystals. J Lumin. 2003;102–103:733–736.
[40] Longo VM, Cavalcante LS, Erlo R, et al. Strong violet–blue light photoluminescence emission at room temperature in SrZrO3: joint experimental and theoretical study. Acta Mater. 2008;56:2191–2202.
[41] Lima RC, Macario LR, Espinosa JWM, et al. Toward an understanding of intermediate- and short-range defects in ZnO single crystals. a combined experimental and theoretical study†. J Phys Chem A. 2008;112:8970–8978.
[42] Rodnyi PA, Khodyuk IV. Optical and luminescence properties of zinc oxide (review). Opt Spectrosc. 2011;111:776–785.
[43] Kern R, Sastrawan R, Ferber J, et al. Modeling and interpretation of electrical impedance spectra of dye solar cells operated under open-circuit conditions. Electrochim Acta. 2002;47:4213–4225.
[44] Walker AB, Peter LM, Lobato K, et al. Analysis of photovoltage decay transients in dye-sensitized solar cells†. J Phys Chem B. 2006;110:25504–25507.
[45] Zaban A, Greenshtein M, Bisquert J. Determination of the electron lifetime in nanocrystalline dye solar cells by open-circuit voltage decay measurements. Chem Phys Chem. 2003;4:859–864.
[46] Wang Q, Ito S, Grätzel M, et al. Characteristics of high efficiency dye-sensitized solar cells†. J Phys Chem B. 2006;110:25210–25221.
[47] Adachi M, Sakamoto M, Jiu J, et al. Determination of parameters of electron transport in dye-sensitized solar cells using electrochemical impedance spectroscopy. J Phys Chem B. 2006;110:13872–13880.
[48] Bisquert J, Fabregat-Santiago F, Mora-Seró I, et al. Electron lifetime in dye-sensitized solar cells: theory and interpretation of measurements. J Phys Chem C. 2009;113:17278–17290.
[49] Bisquert J, Grätzel M, Wang Q, et al. Three-channel transmission line impedance model for mesoscopic oxide electrodes functionalized with a conductive coating. J Phys Chem B. 2006;110:11284–11290.
[50] Bisquert J. Beyond the quasistatic approximation: Impedance and capacitance of an exponential distribution of traps. Phys Rev B. 2008;77:235203–235218.
[51] Schinke C, Hinken D, Bothe K, et al. Determination of the collection diffusion length by electroluminescence imaging. Energy Procedia. 2011;8:147–152.